Solid-State Electronics 199 (2023) 108485

Contents lists available at ScienceDirect

Solid State Electronics

journal homepage: www.elsevier.com/locate/sse

# THz gain compression in nanoscale FinFETs[☆]

Mathias Pech [*], Dirk Schulz

*Chair for High Frequency Techniques, TU Dortmund, Dortmund, Germany*

ARTICLE INFO

*Keywords:*
Computational nanotechnology
Quantum transport
Quantum Liouville
Mode space
FinFET
Gain compression

ABSTRACT

The gain compression and excitation of higher order harmonics in 3 nm wide on-insulator type FinFETs is investigated. The high computational burden related to the time-resolved analysis of such three-dimensional devices is dealt with by applying a mode-space approach onto a Quantum Liouville-type Equation. With this approach an increase in gain compression and higher order harmonic distortion is observed when decreasing the fin height from 5 to 3 nm.

## 1. Introduction

Current interest in analog and mixed signal circuits is as high as ever, with applications ranging from mixers and general systems on chip (SoC) to specialized architectures for high-performance computing (HPC) that can possibly outperform their digital counterparts [1]. Multigate-FETs with Gate-All-Around- (GAA) and Fin-type gate architectures are especially important due to their excellent channel control and ease of integration into stacked transistor structures [2].

For amplifier and mixer applications, time-resolved quantum transport simulations are necessary in order to study the nonlinear behavior of these multigate-FETs. Quantum Liouville-type approaches in particular have been demonstrated to be well suited [3], but have been mostly limited to either stationary or transient but low-dimensional devices in the past (e.g. [4]).

In this contribution, the approach is extended to the three-dimensional regime utilizing a Quantum Liouville-type Equation (QLTE) in order to evaluate the gain compression in FinFETs. To further reduce the computation time, the transport is effectively projected onto the dominant transport direction. This is done by approximating the density matrix in transport direction with an expansion in terms of the eigensolutions of Schrödinger's equation in the confinement direction, the so-called modes [5,6]. The resulting method is called mode-space approach, which enables the efficient and self-consistent transport modeling.

Therefore, the approach to be presented is perfectly suited for the investigation of the charge carrier transport in nanoscale Multigate-FETs in the time-domain. As quantum confinement is inherently included with this method, the impact on RF characteristics, e.g. THz gain compression, can be studied. An increase of nonlinearities as a result of quantum confinement has been predicted in simulations previously, though only a simple harmonic balance method was used [7]. As an example, with our approach this effect is confirmed and can be studied in more detail.

## 2. Quantum transport in mode-space

An appropriate method based on the solution of a Quantum Liouville type equation (QLTE), which is self-consistently solved along with Poisson's equation, is extended to allow an efficient three-dimensional analysis. Ballistic transport and a constant effective mass $m$ is assumed here, though the ansatz presented is perfectly suited for an extension to account for scattering, as well as a spatially varying effective mass. First, Schrödinger's equation in the effective mass- and Hartree approximation

$$\imath\hbar \frac{\partial}{\partial t}\Psi(x,y,z,t) = \left(-\frac{\hbar^2}{2m^*}\nabla^2 + V(\boldsymbol{r})\right)\Psi(x,y,z,t) \tag{1}$$

is solved assuming a carrier confinement in the $yz$-plane and a dominant transport in $x$-direction. This results in modes $m$ described by their wave functions $\psi_m(y,z,t)$ and corresponding subband energies $E_m$. The expansion of the wave function $\Psi$ of Schrödinger's equation in terms of the modes $\psi_m$ leads to the ansatz

$$\Psi_k(x,y,z,t) = \sum_m \varphi_m(x,t)\psi_m(y,z,t), \tag{2}$$

where the expansion coefficients $\varphi_m$ have been introduced. Introducing the coupling terms $K_{mn,1}$ and $K_{mn2}$, the following Schrödinger equations

[☆] The review of this paper was arranged by Francisco Gamiz.

[*] Corresponding author.
*E-mail addresses:* mathias.pech@tu-dortmund.de (M. Pech), dirk2.schulz@tu-dortmund.de (D. Schulz).

https://doi.org/10.1016/j.sse.2022.108485

Available online 19 October 2022
0038-1101/© 2022 Elsevier Ltd. All rights reserved.

result, which can be rewritten for each mode $\psi_m$:

$$\begin{aligned}\imath\hbar\frac{\partial}{\partial t}\varphi_m(x,t) &= \left(-\frac{\hbar^2}{2m_x}\frac{\partial^2}{\partial x^2}+E_m(x,t)\right)\varphi_m(x,t)\\ &-\sum_n \underbrace{\frac{\hbar^2}{m_x}\left(\iint dy\,dz\,\psi_m^\dagger\frac{\partial}{\partial x}\psi_n\right)}_{K_{mn,1}}\frac{\partial}{\partial x}\varphi_n(x,t)\\ &-\sum_n \underbrace{\frac{\hbar^2}{2m_x}\left(\iint dy\,dz\,\psi_m^\dagger\frac{\partial^2}{\partial x^2}\psi_n\right)}_{K_{mn,2}}\varphi_n(x,t).\end{aligned} \tag{3}$$

From here on, only the self-coupling terms $K_{m,1}$ and $K_{m,2}$ corresponding to the diagonal coupling terms $n = m$ are taken into account. For the FinFETs considered in this paper, the self-coupling terms are small in comparison to the other coefficients in (3). As it can be seen from (3), the term for $K_{m,2}$ can be interpreted as an additional potential and thus leads to the idea of introducing the effective potential

$$V_m(x,t) = E_m(x,t) - K_{m,2}(x,t) \tag{4}$$

for each mode $m$. As is the case with the modal Schrödinger Eq. (3), a modal density matrix

$$\rho_m(x,x',t) = \sum_{k_x} f_{3D}\left(E_m(k_x)\right)\varphi_m(x,t)\varphi_m^\dagger(x',t) \tag{5}$$

can be derived [8], which is then inserted into the von-Neumann equation

$$\frac{\partial}{\partial t}\rho_m = -\frac{\imath}{\hbar}\left[\hat{H},\rho_m\right]. \tag{6}$$

After a transformation of the density matrix $\rho_m(x,x')$ onto the center-of-mass coordinates $\chi$ and $\xi$, with the former indicating the transport direction, the following functions

$$\begin{aligned}K^{\pm}_{m,1}(\chi,\xi,t) &= K_{m,1}(\chi+\frac{\xi}{2},t)\pm K_{m,1}(\chi-\frac{\xi}{2},t)\\ B_m(\chi,\xi,t) &= V_m(\chi+\frac{\xi}{2},t)-V_m(\chi-\frac{\xi}{2},t),\end{aligned} \tag{7}$$

are introduced. After applying a Fourier transform in $\xi$ direction, the QLTE in the so-called mode-space can be derived as

$$\begin{aligned}\frac{\partial}{\partial t}f_m(\chi,k,t) = &\left[\left(-\frac{\hbar k}{m_x}+\frac{\imath}{4\hbar}\int\frac{dk'}{2\pi}\tilde{K}^{-}_{m,1}(\chi,k'',t)\right)\frac{\partial}{\partial\chi}\right.\\ &+\frac{\imath}{2\hbar}\int_{-\infty}^{\infty}\frac{dk'}{2\pi}\tilde{K}^{+}_{m,1}(\chi,k'',t)\cdot(\imath k')\\ &\left.+\frac{1}{\imath\hbar}\int_{-\infty}^{\infty}\frac{dk'}{2\pi}\tilde{B}_m(\chi,k'',t)\right]f_m(\chi,k',t).\end{aligned} \tag{8}$$

Here, $k'' = k - k'$ has been introduced and the tilde denotes integral kernels regarding $K_1^{\pm}$ and $B$ similar to those of a prototype function $\tilde{U}$ [9]:

$$\tilde{U}(\chi,k'') = \int d\xi\exp\left(-\imath\left(k''\right)\xi\right)\cdot U(\chi,\xi). \tag{9}$$

The total charge carrier densities and current densities can then be calculated from the modal Wigner functions $f_m$ as discussed in [4].

## 3. Investigation of gain compression in FinFETs

Key parameters regarding the size of the FinFET in question are shown in Fig. 1. Two different FinFETs with a fixed fin width of 3 nm and fin heights of 3 and 5 nm are considered for demonstration purposes. The undoped $In_{0.53}Ga_{0.47}As$ channel is 10 nm long, as is the gate contact. The electron affinity of the channel is $\chi = 4.5$ eV. For the oxide and gate material $SiO_2$ and Ag are chosen, respectively with a metal work function of $\varphi = 4.74$ eV assumed for the latter. The source and drain regions on either end of the device are n-doped with $N_s = N_d = 2\cdot 10^{19}\ cm^{-3}$. The eigenvalue problem resulting from Schrödinger's equation in confinement direction is solved by using the Lanczos algorithm with Dirichlet boundary conditions and the assumption of a spatially varying effective mass. It is solved at each time step in the transient case. The QLTE is discretized utilizing a finite volume scheme as described in [9]. Inflow boundary conditions to model carrier transport in and out of the device are adopted for the mode-space approach [8,10] and a complex absorbing potential is added to avoid nonphysical solutions [11].

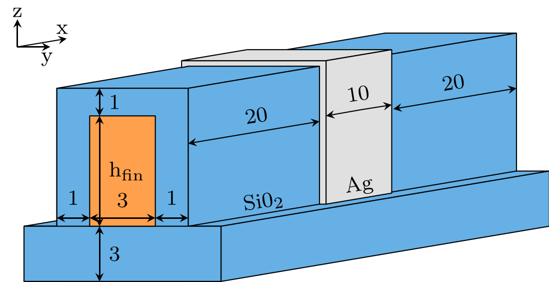


**Fig. 1.** Schematic of the FinFET with all dimensions in nm.

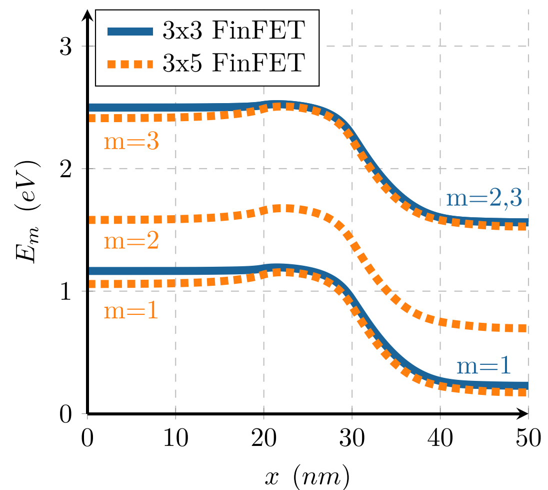


**Fig. 2.** Subband energies belonging to the 3 lowest energy modes along a 3 × 3 nm and a 3 × 5 nm FinFET. The subbands 2 and 3 are nearly degenerate in case of a 3 × 3 nm channel.

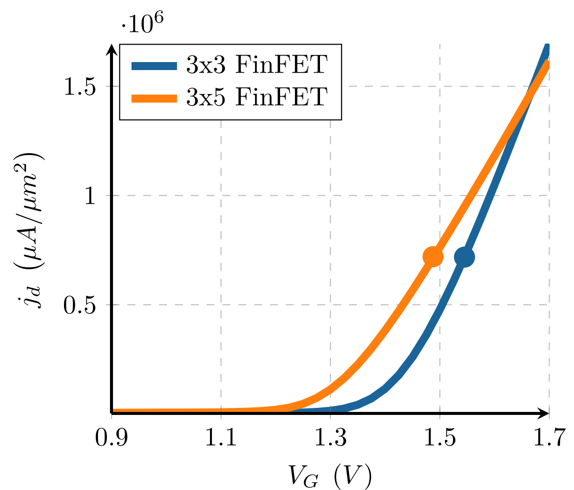


**Fig. 3.** Transfer curves of the FinFETs with marks indicating the operating points.

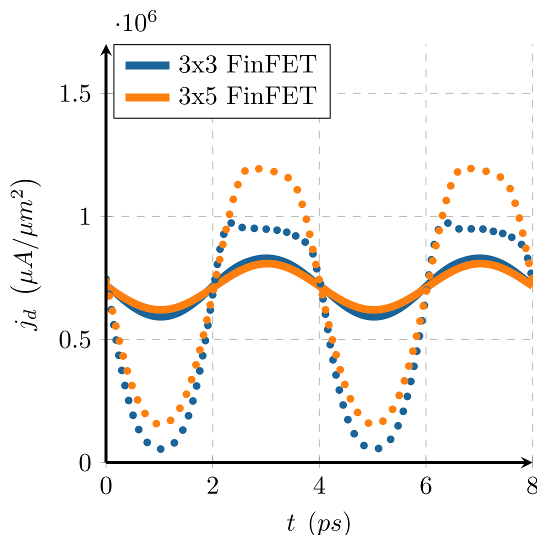


**Fig. 4.** Time-dependent drain-end current density at $V_A = 0.025$ V (—) and $V_A = 0.175$ (⋯).

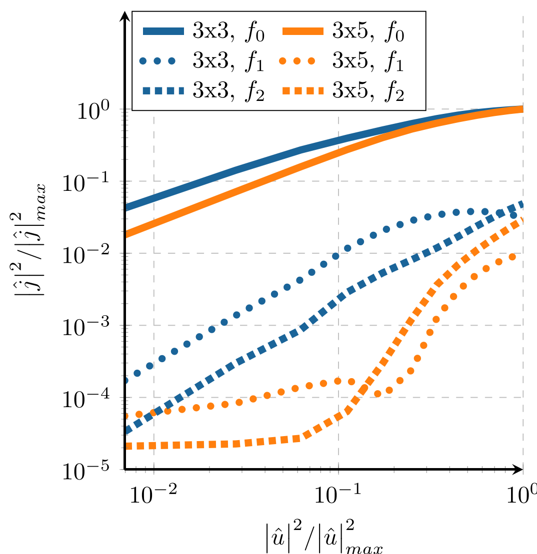


**Fig. 5.** Normalized and squared Fourier coefficients of input (gate voltage) and output (drain-end current density) for the center frequency $f_0$ and the higher order harmonics $f_1$ and $f_2$.

*Stationary results.* In order to determine the operating points $V_0$ for the transient simulations, the stationary QLTE and Poisson's equation are solved iteratively for a constant gate voltage until the Hartree potential $V_H$ of succeeding iterations $n$ and $n-1$ converge in terms of the norm $\|V_H^n - V_H^{n-1}\|$, thus achieving self-consistency. In Fig. 2, a comparison of the resulting subband energies along a $3 \times 3$ nm and a $3 \times 5$ nm FinFETs is shown. As expected, decreasing the fin height leads to higher subband energies, as well as nearly degenerate modes in case of the symmetric $3 \times 3$ nm channel. The transfer behavior is shown in Fig. 3. As it can be seen, the $3 \times 3$ nm FinFET offers a higher gain but has a higher threshold voltage as a result of the higher subband energies

*Transient results.* A harmonic gate voltage of $V_G = V_0 + V_A \cdot \sin(2\pi \cdot f_0 \cdot t)$ with a center frequency $f_0 = 250$ GHz is applied for 18 $ps$ with a time step width of 2 $fs$ and a constant drain source voltage $V_{DS}$ of 1 V. Values from 0 V to 0.3 V are chosen for the amplitude $V_A$ with increments of $\Delta V_A = 0.025$ V. As it is evident from Fig. 4, compression during the positive half-wave takes place sooner in the $3 \times 3$ nm FinFET when compared to the $3 \times 5$ nm FinFET, thus leading to an expected increase in distortion. The drain-end current density is also analyzed in terms of the spectral components at $f_0 = 250$ GHz and the harmonics $f_1 = 500$ GHz and $f_2 = 750$ GHz. As it is evident from Fig. 5, increasing the channel dimensions from $3 \times 3$ nm to $3 \times 5$ nm leads to less excitation of higher order harmonics and higher gain for $f_0$.

## 4. Conclusion

In case of the two FinFETs considered, a decrease of the fin height and thus increase in quantum confinement is shown to lead to a rise in nonlinearities and distortion. Here, further work investigating different channel dimensions and gate architectures is needed in order to optimize amplifier behavior for class-A or class-C operation. Because of the flexibility and efficiency of the mode-space approach, the method can also be extended to atomistic models, the study of transport at low to cryogenic temperatures or spintronic devices, where external fields have to be included.

## Declaration of competing interest

The authors declare that they have no known competing financial interests or personal relationships that could have appeared to influence the work reported in this paper.

## Data availability

Data will be made available on request.

## Acknowledgments

This work was supported by the German Research Funding Association Deutsche Forschungsgemeinschaft (DFG) under Grant SCHU 1016/8. Computing time was provided on the LiDO3 cluster at TU Dortmund, partially funded in the course of the Large-Scale Equipment Initiative by the DFG as project 271512359.

## References


[1] Köppel S, Ulmann B, Heimann L, Killat D. Using analog computers in today's largest computational challenges. Adv Radio Sci 2021;19:105–16. http://dx.doi.org/10.5194/ars-19-105-2021.

[2] Jha N, Chen D. Nanoelectronic circuit design. 2011, p. 1–485. http://dx.doi.org/10.1007/978-1-4419-7609-3.

[3] Weinbub J, Ferry DK. Recent advances in wigner function approaches. Appl Phys Rev 2018;5(4):041104. http://dx.doi.org/10.1063/1.5046663.

[4] Schulz L, Schulz D. Time-resolved mode space based quantum-Liouville type equations applied onto DGFETs. In: 2020 International conference on simulation of semiconductor processes and devices. 2020, p. 331–4. http://dx.doi.org/10.23919/SISPAD49475.2020.9241644.

[5] Venugopal R, Ren Z, Datta S, Lundstrom MS, Jovanovic D. Simulating quantum transport in nanoscale transistors: Real versus mode-space approaches. J Appl Phys 2002;92(7):3730–9. http://dx.doi.org/10.1063/1.1503165.

[6] Ren Z, Venugopal R, Goasguen S, Datta S, Lundstrom M. NanoMOS 2.5: A two-dimensional simulator for quantum transport in double-gate MOSFETs. IEEE Trans Electron Devices 2003;50(9):1914–25. http://dx.doi.org/10.1109/TED.2003.816524.

[7] Dasgupta A, Parihar SS, Kushwaha P, Agarwal H, Kao M-Y, Salahuddin S, et al. BSIM compact model of quantum confinement in advanced nanosheet FETs. IEEE Trans Electron Devices 2020;67(2):730–7. http://dx.doi.org/10.1109/TED.2019.2960269.

[8] Jiang H, Cai W. Effect of boundary treatments on quantum transport current in the Green's function and Wigner distribution methods for a nano-scale DG-MOSFET. J Comput Phys 2010;229(12):4461–75. http://dx.doi.org/10.1016/j.jcp.2010.02.008.

[9] Schulz L, Schulz D. Formulation of a phase space exponential operator for the Wigner transport equation accounting for the spatial variation of the effective mass. J Comput Electron 2020;19. http://dx.doi.org/10.1007/s10825-020-01551-0.

[10] Frensley WR. Boundary conditions for open quantum systems driven far from equilibrium. Rev Modern Phys 1990;62:745–91. http://dx.doi.org/10.1103/RevModPhys.62.745.

[11] Schulz L, Schulz D. Complex absorbing potential formalism accounting for open boundary conditions within the Wigner transport equation. IEEE Trans Nanotechnol 2019;18:830–8. http://dx.doi.org/10.1109/TNANO.2019.2933307.